F. Vignati, A. Guardone
Leading Edge Reflection Patterns for Cylindrical Converging Shock Waves over Convex Obstacles
Physics of Fluids, Vol. 28, N. 9, 2016, 096103 (10 pages)
doi:10.1063/1.4960625

Leading edge reflection patterns for cylindrical converging shock waves over convex obstacles

F. Vignati and A. Guardone

Citation: Physics of Fluids **28**, 096103 (2016); doi: 10.1063/1.4960625
View online: http://dx.doi.org/10.1063/1.4960625
View Table of Contents: http://scitation.aip.org/content/aip/journal/pof2/28/9?ver=pdfcov
Published by the AIP Publishing

PHYSICS OF FLUIDS **28**, 096103 (2016)

Leading edge reflection patterns for cylindrical converging shock waves over convex obstacles

F. Vignati[a] and A. Guardone
Department of Aerospace Science and Technology, Politecnico di Milano, via La Masa, 34 - 20156 Milano, Italy

(Received 18 April 2016; accepted 27 July 2016; published online 21 September 2016)

The unsteady reflection of cylindrical converging shock waves over convex obstacles is investigated numerically. At the leading edge, numerical simulations show the occurrence of all types of regular and irregular reflections predicted by the pseudo-steady theory for planar shock-wave reflections over planar surfaces, although for different combinations of wedge angles and incident shock Mach number. The domain of occurrence of each reflection type and its evolution in time due to shock acceleration and to the non-planar geometry is determined and it is compared to the results of the pseudo-steady theory. The dependence of the reflection pattern on the (local) values of the wedge angle is in good agreement with the pseudo-steady theory. Less complex reflection patterns are instead observed at larger values of the leading edge shock Mach number at which the pseudo-steady theory predicts the occurrence of more complex reflection patterns. *Published by AIP Publishing.* [http://dx.doi.org/10.1063/1.4960625]

I. INTRODUCTION

In recent years, the focusing of converging shock waves has been meeting the interest of the scientific community, thanks to the possibility of concentrating high energy at the focus point, and therefore attaining high pressure and temperature locally. The applications include large-scale energy production,[1] medical treatments,[2] and a number of theoretical physics studies.[3] Unfortunately, as it is well known,[4–6] cylindrical and spherical converging shock waves suffer from surface instabilities. However, if on one hand the intrinsic instability of free implosions often makes them unsuitable for applications, on the other hand it also represents an opportunity, in that surface instabilities can be possibly used to alter the shock wave shape into a more stable one. A very promising stabilization method consists in the so-called *shock reshaping*, i.e., the modification of the shock front shape induced by the forced interaction between the shock and a number of obstacles placed along its propagation path. The shock front shape is eventually modified into a more stable one, thanks to the multiple reflections over the obstacle surfaces.[7]

Several works demonstrate that the combination between the shock Mach number and the geometry of the obstacle has a relevant influence over shock reflections.[8–11] As it is well known, indeed, the interaction between shock waves and solid surfaces results in a number of different reflection types. Most theoretical works on shock reflections are based on the self-similarity of the phenomenon. One of the relevant problems concerns the so-called *pseudo-steady* reflections, i.e., the diffraction of planar shock waves propagating at constant speed by planar wedges. In pseudo-steady interactions, the observed patterns depend only on the incident shock Mach number M_s and on the obstacle wedge angle θ_w^{LE}, see Figure 5, which are both constant for planar waves and obstacles. Patterns originating from pseudo-steady interactions consist of a *Regular Reflection* (RR) or an *Irregular Reflection* (IR).[12] The main difference between the two classes of reflections consists in the number of involved waves: a regular reflection includes only the incident shock and the reflected wave, whereas a further shock wave forms an irregular reflection. Since the pioneering

[a]Electronic mail: federica.vignati@polimi.it

work of Courant and Friedrichs,[13] the second group was assumed to consist of *Mach Reflections* (MRs) only. The MR is a peculiar flow configuration including an incident shock, a reflected shock wave, a Mach stem, and a slip line—the latter necessary to the consistency of the system—all intersecting at the so-called *Triple Point* (TP). According to Courant and Friedrichs,[13] when the triple point moves away from the reflecting surface, the reflection is Direct (DiMR). A Direct Mach Reflection can be a *Single* (SMR), (*Pseudo*) *Transitional* ((P)TMR),[14] or *Double* (DMR)[15,16] Mach Reflection. The distinction among the diverse types of Mach reflection is performed on the basis of the complexity of the structure resulting from the reflection, as described in the complete overview by Ben-Dor,[17] along with transition criteria.

On the contrary, irregular reflections differ from Mach reflections, because of the occurrence of an irregular, SMR-like reflection pattern, which is usually observed in the diffraction of weak shock waves by extremely thin wedges. In these conditions, the diffraction of a Mach reflection is excluded by theoretical models. This apparent contradiction, named the *von Neumann paradox*,[18] was solved with the introduction of an additional kind of non-Mach-type irregular reflection, namely, the *von Neumann reflection (vNR)*.[19,20] Further reflection types were discovered from the study of the reflection of weak shock waves,[21] e.g., the *Vasil'ev reflection*[22] and the *Guderley reflection*.[23] Based on theoretical considerations and on experimental and numerical evidences,[24] the reflections listed above are the only possible detectable configurations in the reflection of planar shock waves at the leading edge of straight wedges.

Analytical criteria derived for pseudo-steady shocks, e.g., length scale criterion,[25] mechanical equilibrium criterion,[26] sonic criterion[27,28] (an improvement of the detachment criterium, see Ref. 29), allow us to determine the occurring reflection type depending on the combination between the incident shock Mach number and the leading edge wedge angle. The generalization of pseudo-steady results obtained for planar shock waves interacting with planar geometries to the case of curved wave fronts interacting with curved wall is not trivial. Indeed, the non-constant propagation speed of converging shock waves[30,31] and the positive convexity of both the shock and the obstacle make the reflection of implosions genuinely unsteady. To the authors' knowledge, no complete studies of the interaction of curved shock waves with curved obstacles is available.

This work aims at investigating the reflection patterns generated by the interaction of a cylindrical converging shock wave with a circular-arc obstacle. Numerical simulations are performed on a set of configurations, including different levels of incident shock Mach number M_s, obstacle thickness-to-chord ratio t/c, and leading edge radius-to-chord ratio r_{LE}/c. The latter is a novel parameter, that is not relevant in the self-similar case (see Sec. II for details), because it influences both the shock curvature and the shock wave intensity at the impingement point.[30] In the numerical experiments, the shock propagates in dilute air, modeled as an ideal gas with constant specific-heat ratio $\gamma = 1.4$. Viscous phenomena are assumed to be confined in the boundary layer,[32] whose thickness is considered negligible with respect to the reference scales of the problem. Therefore, results are disengaged from the spatial scale. The software adopted for the numerical simulation of the reflections is the FlowMesh code, a solver for Euler equations developed within the Department of Aerospace Science and Technology of Politecnico di Milano.[33,34]

Numerical results are compared to reflection types predicted by self-similar theory[17] to gain further insight into the behaviour of genuinely unsteady reflections and to point out the similarities and the differences between the two cases. Indeed, as pointed out by Ben-Dor and Takayama,[35] some unsteady shock diffractions can be approximately represented as a sequence of pseudo-steady reflection.

This paper is structured as follows: the definition of the investigated problem and the set of parameters are outlined in Sec. II. The features of the numerical simulations and the methodology are briefly reported in Sec. III. The numerical result, i.e., the partition of the plane M_s^{LE}–θ_w^{LE} on the basis of the reflection (regular or Mach-type), is described in Sec. IV, and it is duly discussed. Conclusions and final considerations are reported in Sec. V.

II. SHOCK/OBSTACLE CONFIGURATIONS

As it is well known, in ideal constant-specific-heat ideal gases, pseudo-steady reflections of planar shock waves over planar obstacles are completely determined only by the wedge angle θ_w

and by the incident shock Mach number, which are both assumed to remain constant.[17] In the reflection of planar shock waves over circular-arc obstacles,[36] the sole leading edge wedge angle θ_w^{LE} was proved to be insufficient to define the type of leading edge reflection and its evolution during time. In the same work,[36] also the obstacle radius of curvature R_o was found to be influential on the evolution of the shock wave reflection. This implies that characteristic lengths must be introduced to deal with unsteady shock wave reflections. In this work, all the geometrical variables are made dimensionless with the semi-chord length. All the obstacles are assumed to be defined by a circular arc with a constant semi-chord c = 1 and variable semi-thickness t, so that the obstacle geometry is fully defined by the parameter t/c only. Therefore, θ_w^{LE} and R_o both depend only on the value of t/c as follows:

$$\begin{aligned} \frac{R_o}{c} &= \frac{1}{2}\left[t/c + \frac{1}{t/c}\right], \\ \theta_w^{LE} &= \frac{\pi}{2} - \arctan\left(\frac{1}{t/c} - t/c\right). \end{aligned} \tag{1}$$

The computational domain and the geometry are sketched in Fig. 1. The geometry of the obstacle is taken from the test rig described in Ref. 8. The configuration includes an array of 8 circular-arc obstacles with a thickness-to-chord ratio $t/c = 0.14$ and symmetrically arranged at a distance $r_{LE}/c = 2.8$ from the origin (0,0). According to Ref. 8, the Mach number of the incident shock wave is $M_s^{LE} = 2.7$, and it is evaluated when the shock is about to approach the obstacle leading edge, i.e., at $r/c = r_{LE}/c + 0.4$. The same parameters and operating conditions of Ref. 8 were adopted also in Ref. 37, which focuses on a parametric study of the shock reshaping by means of numerical simulations.

In this work, the value of t/c is varied over thirteen levels as follows:

$$t/c = 0.07 \cdot (1, 2, 3, 4, 5, 6, 6.5, 7, 8, 9, 11, 13), 1, \tag{2}$$

where the latter value, $t/c = 1$, corresponds to the cylindrical case.

In the numerical simulations, the shock wave is generated by imposing a circumferential pressure and density step far upstream the obstacle leading edge on still gas. The pressure and density step is located at a radial distance of $10c$ from the origin. This distance was chosen to guarantee self-similar convergence of the shock waves.[30] A three-wave system is generated, i.e., a shock wave moving inwards, a contact discontinuity following the shock wave, and a rarefaction wave moving outwards. The internal pressure P_i and density ρ_i are kept constant for all the simulations, whereas the initial external pressure is $P_e = \beta_P P_i$. The parameter β_P, namely, the initial pressure ratio, is the

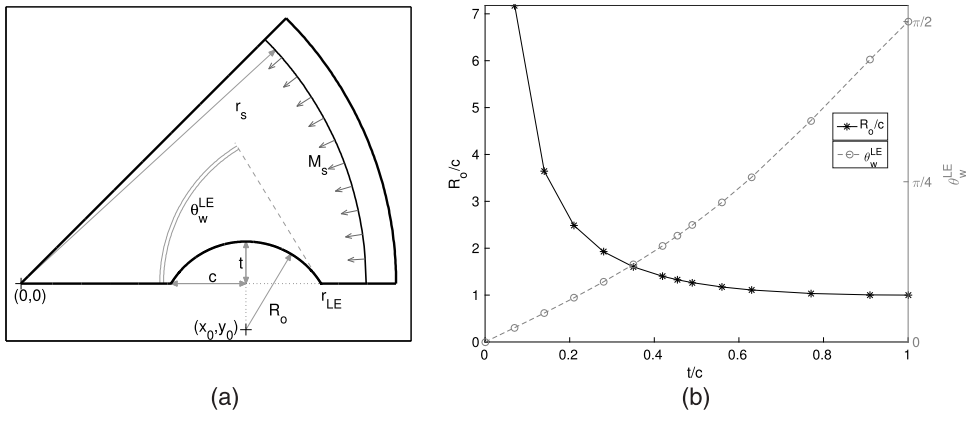

FIG. 1. (a) Sketch of the computational domain and of geometrical features. A half-obstacle is represented, with leading-edge radius r_{LE}/c and leading-edge wedge angle θ_w^{LE}, depending on the thickness-to-chord ratio t/c. The obstacle profile is a circular-arc, with center in (x_0, y_0) and radius R_o. The shock is depicted before the reflection, at a radius $r_s > r_{LE}$, converging towards the focus point (0, 0) with a Mach number M_s. In the plot, r_s indicates the distance from the origin (0,0) and R_o is the distance from the center of the circular-arc obstacle. (b) Dependence of R_o/c and of θ_w^{LE} on the parameter t/c in the considered cases.

TABLE I. Test matrix for the numerical experiments. Considered parameters are the thickness-to-chord ratio t/c, the radial coordinate of the obstacle leading edge r_{LE}/c, and the initial pressure ratio β_P. In all tests, the operating fluid is air in standard conditions, with $\gamma = 1.4$.

Thickness-to-chord ratio	t/c	0.07, 0.14, 0.21, 0.28, 0.35, 0.42, 0.445, 0.49, 0.56, 0.63, 0.77, 0.91, 1
Chord-normalized leading edge radius	r_{LE}/c	2.8, 5.6, 7
Initial pressure ratio	β_P	11, 16, 27, 36, 48, 60, 75, 90, 110, 130

controlled parameter to characterize the diverse shock waves. The shock intensity, indeed, is proportional to the value of M_s evaluated at $r/c = r_{LE} + 0.4$, namely, at $0.4c$ upstream the obstacle leading edge. Note that the quantities β_P and M_s^{LE} are not interchangeable, because the Mach number of a wave generated by a given β_P changes in space and time in accordance to Guderley's law.[30] The values of β_P are chosen in order to have equally distributed M_s^{LE} over ten levels, from 2.2 to 6.7, at $r_{LE}/c = 2.8$. The dependence of M_s^{LE} on β_P for different values of r_{LE}/c for converging shock is reported in Figure 15 of Ref. 37.

The obstacle is located in three different positions, corresponding to $r_{LE}/c = 2.8$, 5.6, and 7. The effect of the leading edge radius on the reflection is two-fold: by varying r_{LE}/c, the curvature of the shock wave at the obstacle leading edge is modified and also the value of M_s^{LE} obtained at a given β_P is modified. The numerical experiments are distributed on a full factorial design[38] for an overall number of 390 treatments, see Table I.

III. NUMERICAL SIMULATIONS OF CONVERGING SHOCK WAVES

Numerical simulations are performed by means of a multi-domain procedure[39] consisting of two steps.

The first step concerns the shock onset from an initial pressure difference in the so-called far field. The initial condition consists in two uniform regions, i.e., the internal and the external one. In the internal region, the pressure is $P_i = 10^4$ Pa and the temperature is $T_i = 298.15$ K, in accordance to Ref. 37. In the dilute conditions of interest, the polytropic—namely, constant specific heats—ideal gas model is used to describe the thermodynamics of air. Therefore, the internal density is computed as $\rho_i = P_i/(RT_i)$, where R is the mass-averaged gas constant $R = \mathcal{R}/\sum_{h=1}^{n_c} M_h z_h$, with n_c the number of components of the gas mixture, M_h the molecular mass, and z_h the molar fraction of the hth component. Air is modeled as a binary mixture of mostly diatomic gases, i.e., nitrogen (78%) and oxygen (21%), and therefore, $R = 287.046$ J/(kg K).

The external pressure is $P_e = \beta_P P_i$; the external density is computed from the Rankine-Hugoniot conditions for polytropic ideal gas. Before the shock-obstacle interaction, the shock exhibit cylindrical symmetry and therefore the solution is computed by means of one-dimensional Euler solver in cylindrical coordinates,[40] which allows a reduced computational cost with respect to the solution of the two-dimensional problem. The one-dimensional radial simulation ends when the shock wave is about to approach the obstacle leading edge.

The one-dimensional solution is then interpolated over a two-dimensional domain including the region of interaction to initialize the calculation of the shock-obstacle interaction, i.e., the second step of the multi-domain approach. The shock reflection over the obstacle leading edge is simulated by means of the FlowMesh code, a Finite Volume solver for unsteady Euler's equation developed at the Department of Aerospace Science and Technology of Politecnico di Milano.[33,34] The code uses high-resolution flux and backward Euler method for the time integration of the equations. The reader is referred to Refs. 39 and 37 for a detailed description of the multi-domain approach.

Reference 37 also reports the assessment on the space and time discretization for the shock-obstacle interaction problem of interest here. The pressure along the obstacle and the temperature

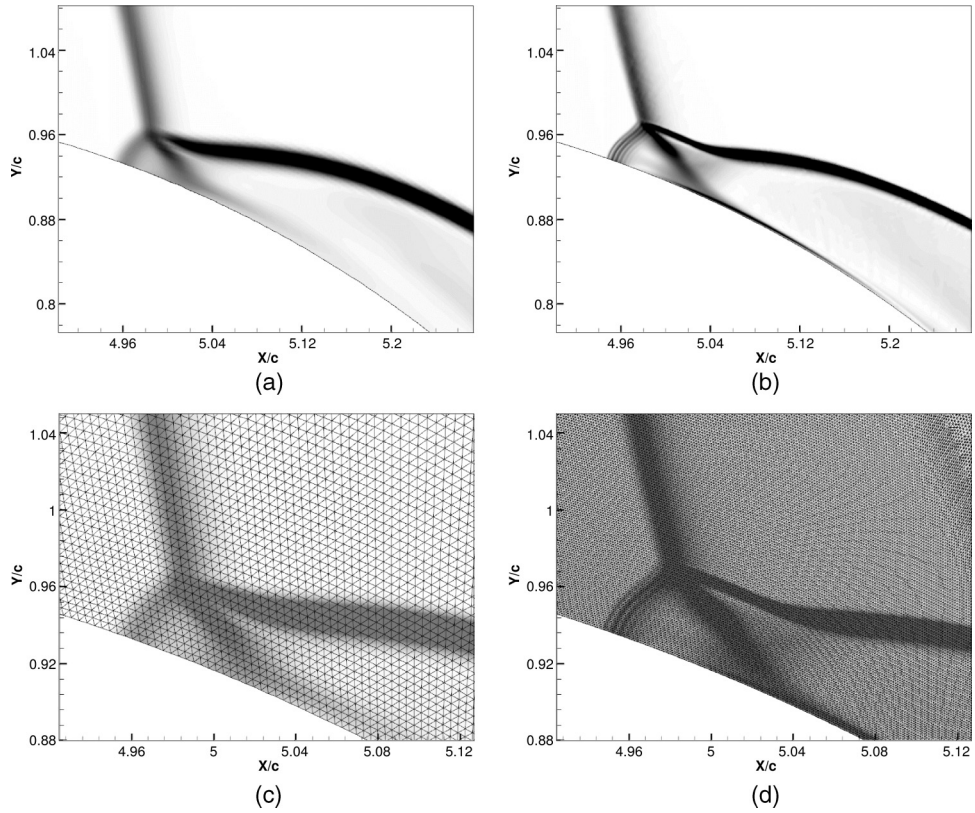

FIG. 2. Numerical Schlieren in correspondence with a circular obstacle leading edge: (a) uniform grid and (b) local refinement, with the corresponding meshes in (c) for uniform $\Delta x = 0.01$ and (d) for refined Δx up to 0.001 ($\beta_P = 130$, $t/c = 1$, $r_{LE} = 14$).

at the focus point of the imploding shock are computed in Ref. 37 using diverse grid spacings and time steps. Since the same configurations (obstacle shape, thickness, position, and shock Mach number) are examined in this work, the same space and time discretizations are adopted. Therefore, calculations are performed on a fixed grid with normalized node spacing $\Delta x = 0.002$, and hence, the number of nodes of two-dimensional meshes ranges between 200 000 and 500 000 depending on r_{LE}/c. An *a priori* mesh refinement is performed at the obstacle leading edge to capture the details of the shock diffraction. In the present work, the numerical grid was assessed also against the resolution of flow features, including the complex triple-point configuration. Figure 2 shows the numerical Schlieren in the close proximity of the obstacle leading edge for uniform ($\Delta x = 0.01$) and locally adapted (with a minimum spacing of $\Delta x = 0.001$) grids. In both cases, the reflection pattern is a transitional Mach reflection, though the finer grid allows for a more detailed representation of the flow features. Numerical experiments with finer grids do not show significant improvements over the locally adapted one, in terms of resolution of the flow features. A similar procedure is followed to determine the time step $\Delta\tau$, by analysing the leading edge patterns obtained from different values of $\Delta\tau$. The adopted time step is $\Delta\tau/\tau_{ref} = 1.8 \times 10^{-4}$. τ_{ref} is the reference time, and it is computed as $c/(2.5\sqrt{T_i R})$.

IV. NUMERICAL EXPERIMENTS

A. Leading edge reflection patterns

According to available theoretical and experimental results, the reflection of a planar shock wave over either planar or curved obstacles can result in multiple reflections patterns.[17] The main

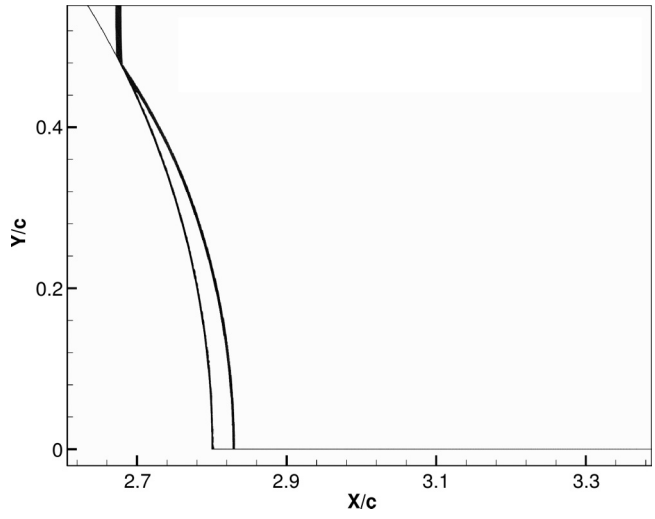

FIG. 3. Numerical Schlieren image highlighting a regular reflection of a cylindrical implosion with $M_s^{LE} = 6.7$ over a cylindrical obstacle with $r_{LE}/c = 2.8$.

subdivision concerns the number of waves belonging to the structure that arises within the reflection and their interactions.

When only the initial, i.e., the incident, and a single reflected shock are observed, the reflection is termed regular; these two waves merge into a point belonging to the reflecting surface called reflection point. Usually, a regular reflection occurs for very large values of θ_w^{LE}, as illustrated in Fig. 3, which depicts the numerical simulation of the reflection of a shock wave with $M_s^{LE} = 6.7$ over a cylindrical obstacle with $\theta_w^{LE} = \pi/2$.

If a third shock—a *Mach stem*—and a slip line are observed, the reflection is named Mach reflection, and the reflection point becomes a triple point. Fig. 4 reports numerical results of four simulations of the reshaping of cylindrical shocks with $M_s^{LE} = 6.7$ in $r_{LE}/c = 2.8$ over variable ℓ/c obstacles. For all four depicted configurations, the reflection is of Mach type, but the patterns behind the triple point differ from each other. Mach reflections are further divided into diverse sub-categories, depending on the complexity of the resulting structure, including Double Mach Reflections (DMRs, (a)), Transitional Mach Reflections (TMRs, (b)), Pseudo-Transitional Mach Reflection (PTMR, (c)), and Single Mach Reflection (SMR, (d)).[17] The numerical simulations suggest that the lower the value of ℓ/c, the less complex the resulting shock structure.

It is worth noticing that all the reflections reported in Figs. 3 and 4 concern incident shock waves with $M_s^{LE} = 6.7$ in $r_{LE}/c = 2.8$, corresponding to $\beta_P = 130$, and differ from each other only because of different values of ℓ/c. This is in accordance with pseudo-steady results: in general, for a given M_s^{LE}, the lower is ℓ/c, the less complex is the resulting shock structure.

The theory of pseudo-steady shocks predicts that for small perturbations, namely, both weak shocks and thin wedges, the three-shock structure resulting from the reflection fades towards a structure similar to a MR, but with a gradual bending of the incident shock and of the Mach stem rather than a single point of intersection, that is indeed the TP. This kind of flow structure is known as von Neumann reflection (vNR).[19,20] Even though the present numerical experiments are designed to obtain $M_s > 2$ at $r_{LE}/c = 2.8$, the aforementioned extension of the factorial design to $r_{LE}/c > 2.8$ produced some configurations with an incident shock Mach number lower than 2, generating a weak reflection on obstacles with the lowest ℓ/c. The grid resolution in this case is not sufficient to determine whether the observed configuration is a vNR or a SMR (or a different type of weak reflection, see the discussion in Ref. 37) and to perform a detailed analysis of the complex region of the equivalent TP.[41] For this reason, this work only focuses on strong shocks, and the occurrence of the vNR-like structure is only reported for completeness.

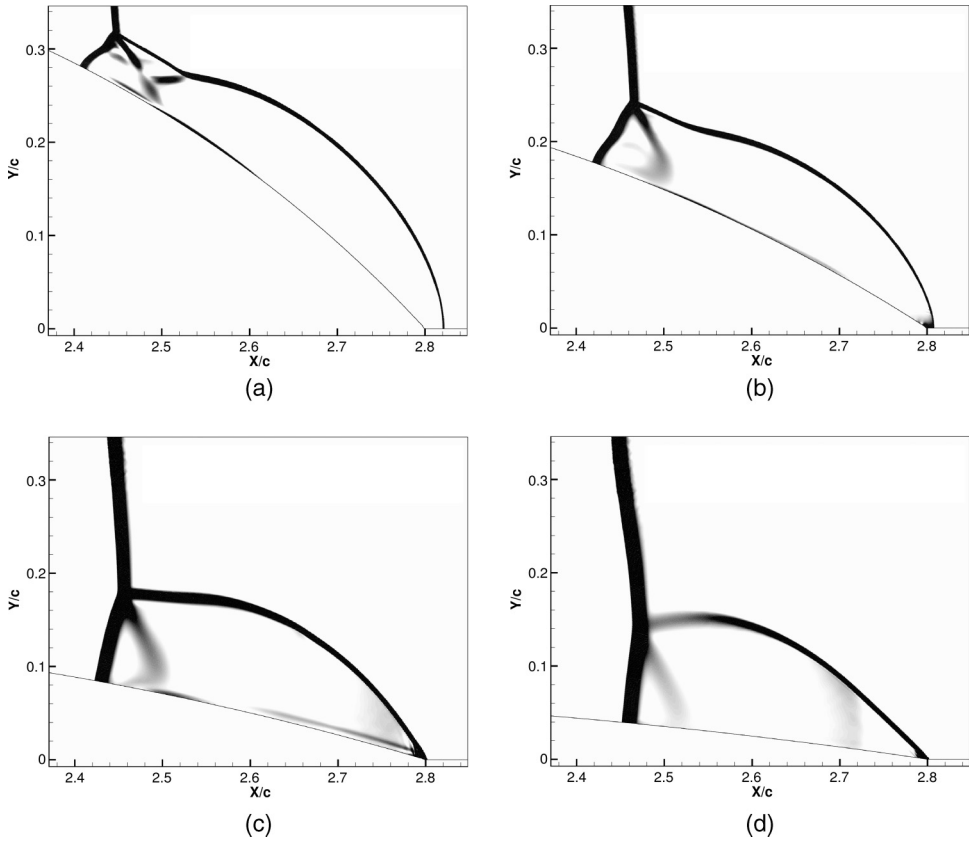

FIG. 4. Reflection patterns detected in the diffraction of cylindrical implosions over circular-arc obstacles: (a) $t/c = 0.42$ DMR, (b) $t/c = 0.28$ TMR, (c) $t/c = 0.14$ PTMR, and (d) $t/c = 0.07$ SMR are obtained for $M_s^{LE} = 6.7$ at $r_{LE}/c = 2.8$.

B. Partition of the M_s^{LE}–θ_w^{LE} plane

The classical approach to the determination of shock reflection types, adopted also for steady, pseudo-steady, and some unsteady cases (see, e.g., Ref. 42), consists in classifying the shock configurations depending on the shock wave Mach number M_s and on the obstacle wedge angle θ_w. Since in these cases both M_s and θ_w are constant, these two parameters alone are sufficient to fully identify each configuration. On the contrary, during the reflection of converging shock waves over curved obstacles, both M_s and θ_w change locally. In the present study, the reference values of M_s and θ_w are the values of the shock Mach number at $r_{LE}/c + 0.4$ and of the leading-edge wedge angle, M_s^{LE} and θ_w^{LE}, respectively. Each combination of leading edge shock Mach number M_s^{LE} and leading edge wedge angle θ_w^{LE} results in one of the aforementioned reflection types, and therefore, the plane is partitioned along transition lines, in accordance with classical criteria.[25,26,29]

The same classification is applied here for the first time to the diffraction of cylindrical shocks over circular-arc obstacles: the diverse types of leading edge reflections are reported in Fig. 5, arranged by M_s^{LE} and θ_w^{LE}. The first parameter includes the effects of β_P and r_{LE}/c. The intensity of the shock wave depends on the initial pressure ratio β_P and, in accordance with Guderley's theory, the shock speed increases as the shock wave approaches the focus point. Therefore, the Mach number at the leading edge reflection of each shock wave depends also on the radius of the obstacle leading edge. According to (1), the value of θ_w^{LE} depends only on t/c, and therefore, the influence of all the geometrical factors and operating conditions is accounted for. Note that in Fig. 5 data appear to be more concentrated for $M_s^{LE} \in [2,3]$ because for $\beta_P = 11, 16, 27$ the reflection types are plotted also for $r_{LE}/c = 5.6$ and $r_{LE}/c = 7$.

In Fig. 5, full lines represent the partitions of the plane in diverse regions, corresponding to the reflection types according to the pseudo-steady theory. The partitions lines are computed from to the

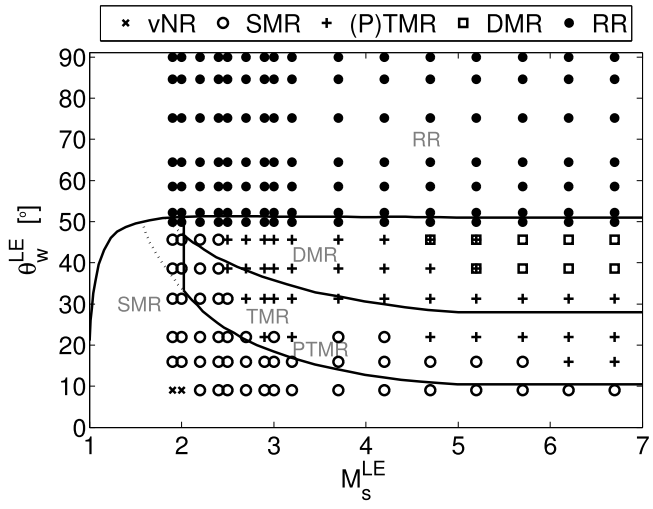

FIG. 5. Leading edge reflection types. Full lines represent the partition of the plane according to the length-scale criterion for pseudo-steady reflections. The diverse symbols represent diverse reflection types of converging shock waves over circular-arc obstacles, as resulting from numerical simulations. Where two different symbols overlap, the distinction between the two types of reflection is not clear.

length scale criterion.[24,25] The theory was developed under the pseudo-steadiness assumption, and therefore, it does not strictly apply to this context, where two unsteadiness sources are present, i.e., the obstacle profile and the shock curvature. However, as suggested in several works,[35,36] to a first approximation, the unsteady shock diffraction can be interpreted also as a sequence of steady states. All the reflection types predicted by pseudo-steady criteria for the explored range of M_s^{LE} and θ_w^{LE} can be observed also in the investigation of the interaction between curved shocks and obstacles: regular reflections and single, (pseudo-)transitional, and double Mach reflections. The validity of the pseudo-steady representation in describing the diffraction of a shock wave over a wedge is confirmed by the present numerical simulations.

The comparison between the transition lines of pseudo-steady reflections and numerical results in Fig. 5 reveals that for a given θ_w^{LE}, the M_s^{LE} which separates two diverse regions on the plane for unsteady reflections is higher than the corresponding pseudo-steady case. The occurrence of this shift at each transition suggests that, in each region of the plane, the less complex reflection type in the unsteady case occurs even in the range of Mach numbers where the more complex type would be expected according to pseudo-steady theories. On the contrary, if M_s^{LE} is fixed and θ_w^{LE} is increased, the observed configuration is the same as the one predicted by the pseudo-steady theory. Indeed, both the qualitative trend of transition lines and quantitative values of the transition wedge angles remain the same as for pseudo-steady shock reflections. In the pseudo-steady case, the transitional wedge angles as function of M_s^{LE} show a convergence towards an asymptotic value for increasing M_s^{LE}.[17] With reference to Fig. 5, the above asymptotic behaviour of the partition lines can be observed also in the reflection of cylindrical shocks over circular-arc obstacles. Therefore, at a given M_s^{LE}, the comparison is performed between the asymptotic value of the partition lines and the asymptotic value of the boundaries of the domains of occurrence of each reflection type. Unlike the comparison at fixed θ_w^{LE}, this comparison at fixed M_s^{LE} shows good accordance with pseudo-steady results. In particular, the asymptotic value of θ_w^{LE} separating the onset of regular and Mach reflections at the leading edge is termed *critical leading wedge angle* or θ_w^{cr}: for the reflection of cylindrical converging shocks over circular-arc obstacles, it is observed that θ_w^{cr} remains close but slightly smaller than the corresponding one for pseudo-steady reflections, which ranges from 49° to 51°, depending on the adopted criterion. This means that the onset of an unsteady Mach reflection at the leading edge is impossible when $\theta_w^{LE} > 48°$. In this case, when a regular reflection occurs at the leading edge, a transition from regular to Mach reflection is observed to take place during the shock propagation along the obstacle, similarly to what is observed in Ref. 36 for the reflection of

planar shock waves over curved obstacles, and it will be discussed in future works for the case of converging shock waves.

In Fig. 5, the two reflections in the bottom-left of the M_s^{LE}–θ_w^{LE} plane are possibly either single Mach reflections or von Neumann reflections. However, due to the uncertainty about the possibility of obtaining von Neumann reflection for the considered parameters (see Ref. 37 for details), no further comments is possible in the present work.

V. COMMENTS AND CONCLUSIONS

Numerical simulations of cylindrical converging shock waves interacting with circular-arc obstacles were performed for air in dilute conditions, under the constant-specific-heat ideal-gas model. A multi-domain approach was used to interface two solvers for the Euler equations: a one-dimensional cylindrical one—for the simulation of the cylindrical shock onset and propagation—and a two-dimensional solver for Euler equations in Cartesian formulation for the simulation of the shock-obstacle interaction.

The effects of the shock Mach number and of the obstacle thickness and distance from the focus point on the reflection type at the leading edge of the obstacle were considered. The pseudo-steady theory was used as a reference for the local features of the reflections. All the reflection types which are known to occur in the pseudo-steady case were observed here for the first time also in the diffraction of cylindrical converging shock waves over circular-arc obstacles.

Numerical results show the occurrence of regular reflections and of single, (pseudo-)transitional, and double Mach reflections in the diffraction of strong converging shock waves over circular-arc obstacles.

The occurrence of each reflection type is associated to two parameters, i.e., the shock wave Mach M_s^{LE} 0.4 chord upstream of the obstacle and the leading-edge slope θ_w^{LE}. A partition of the plane $M_s^{LE} - \theta_w^{LE}$ in four regions was obtained, showing on the one hand a good accordance with pseudo-steady results for the values of θ_w^{LE} triggering the transitions between the various reflections—including θ_w^{cr}—but, on the other hand, a relevant difference in the values of transitional M_s. In particular, in each region of the plane, the less complex reflection type in the unsteady case is observed even in the range of Mach numbers where the more complex type would be expected according to pseudo-steady theories.

Besides the understanding of fundamental properties of curved shock reflections over curved geometry, the present results can be used to provide a guideline in selecting the suitable obstacle configuration to achieve the envisaged shock polygonalisation in shock-reshaping applications.

A final remark concerns the choice of the range of variation of each parameter: r/c is varied from a value very close to zero up to one, and therefore, all the possible thickness effects were accounted for. The shock wave Mach number at the leading edge is varied over the largest range, too. Indeed, for shocks stronger than the explored ones, high temperature effects become non-negligible, and therefore, the polytropic ideal gas model cannot apply. On the contrary, if weaker shocks are considered, it is necessary to keep into account the different physics of weak shock reflections.[21] Moreover, we note that the present results depend on the chosen gas (air) via the constant specific-heat-ratio γ. The influence of γ on the reshaping of cylindrical shock by means of circular-arc obstacles was studied by Kjellander *et al.*[8] by comparing experiments with air ($\gamma = 1.4$) and argon ($\gamma = 5/3$) in terms of integral parameters only. The influence of γ on the partition of the M_s^{LE}–θ_w^{LE} plane in Figure 5 is left for future investigations.

[1] S. Atzeni and J. Meyer-ter-vehn, *The Physics of Inertial Fusion: Beam Plasma Interaction, Hydrodynamics, Hot Dense Matter* (Oxford University Press, 2004).
[2] P. O. K. Krell, *History of Shock Waves, Explosions and Impact - A Cronological and Biographical Reference* (Springer Science & Business Media, 2008).
[3] B. P. Barber and S. J. Putterman, "Light scattering measurements of the repetitive supersonic implosion of a sonoluminescing bubble," Phys. Rev. Lett. **69**, 3839–3842 (1992).
[4] R. W. Perry and A. Kantrowitz, "The production and stability of converging shock waves," J. Appl. Phys. **22**, 878–886 (1951).
[5] V. A. Thomas and R. J. Kares, "Drive asymmetry and the origin of turbulence in an ICF implosion," Phys. Rev. Lett. **109**, 075004 (2012).

[6] V. A. Smalyuk, D. T. Casey, D. S. Clark, M. J. Edwards, S. W. Haan, A. Hamza, D. E. Hoover, W. W. Hsing, O. Hurricane, J. D. Kilkenny, J. Kroll, O. L. Landen, A. Moore, A. Nikroo, L. Peterson, K. Raman, B. A. Remington, H. F. Robey, S. V. Weber, and K. Widmann, "First measurements of hydrodynamic instability growth in indirectly driven implosions at ignition-relevant conditions on the National Ignition Facility," Phys. Rev. Lett. **112**, 185003 (2014).
[7] D. W. Schwendeman and G. B. Whitham, "On converging shock waves," Proc. R. Soc. A **413**, 297–311 (1987).
[8] M. Kjellander, N. Tillmark, and N. Apazidis, "Thermal radiation from a converging shock implosion," Phys. Fluids **22**, 046102 (2010).
[9] N. Apazidis, M. Kjellander, and N. Tillmark, "High energy concentration by symmetric shock focusing," Shock Waves **23**, 361–368 (2013).
[10] V. Eliasson, N. Apazidis, and N. Tillmark, "Controlling the form of strong converging shocks by means of disturbances," Shock Waves **17**, 29–42 (2007).
[11] V. Eliasson, "On focusing of shock waves," Ph.D. dissertation, Department of Mechanics, KTH, Sweden, 2007.
[12] E. Mach, "Über den verlauf von funkenwellen in der ebene und im raume," Sitzungsbr. Akad. Wiss. Wien **78**, 819–838 (1878).
[13] R. Courant and K. O. Friedrichs, *Supersonic Flow and Shock Waves* (Wiley Inc., New York, 1948).
[14] L. G. Smith, "Photographic investigation of the reflection of plane shocks in air," OSRD Report 6271, Office of Scientific Research and Development, Washington, DC, 1945.
[15] D. R. White, "An experimental survey of the Mach reflection of shock waves," Technical Report II-10, Department of Physics, Princeton University, 1951.
[16] G. Ben-Dor, "Relations between first and second triple point trajectory angles in double mach reflection," AIAA J. **19**, 531–533 (1981).
[17] G. Ben-Dor, *Shock Wave Reflection Phenomena* (Springer, 1995).
[18] G. Birkhoff, *Hydrodynamics, A Study of Logic and Similitude*, 1st ed. (Princeton University Press, Princeton, NJ, 1950).
[19] M. J. Lighthill, "The diffraction of blast. I," Proc. R. Soc. A **198**, 454–470 (1948).
[20] P. Colella and L. F. Henderson, "The von Neumann paradox for the diffraction of weak shock waves," J. Fluid Mech. **213**, 71–94 (1990).
[21] E. W. Skews and J. T. Ashworth, "The physical nature of weak shock wave reflection," J. Fluid Mech. **542**, 105–114 (2005).
[22] E. I. Vasilev, "Four-wave scheme of weak Mach shock wave interaction under von Neumann paradox conditions," Fluid Dyn. **34**, 421 (1999).
[23] K. G. Guderley, *The Theory of Transonic Flow* (Pergamon, New York, 1962), pp. 147–149.
[24] H. Li and G. Ben-Dor, "Reconsideration of pseudo-steady shock wave reflections and the transition criteria between them," Shock Waves **5**, 59–73 (1995).
[25] H. G. Hornung, H. Oertel, and R. J. Sandeman, "Transition to Mach reflexion of shock waves in steady and pseudosteady flow with and without relaxation," J. Fluid Mech. **90**, 541–560 (1979).
[26] L. F. Henderson and A. Lozzi, "Experiments on transition of Mach reflection," J. Fluid Mech. **68**, 139–155 (1975).
[27] J. von Neumann, *Collected Works* (Pergamon Press, 1963), Vol. 6, pp. 238–299.
[28] S. Itoh, N. Okazaki, and M. Itaya, "On the transition betwen regular and Mach reflection in truly non-stationary flows," J. Fluid Mech. **108**, 383–400 (1981).
[29] G. D. Lock and J. M. Dewey, "An experimental investigation of the sonic criterion for transition from regular to Mach reflection of weak shock waves," Exp. Fluids **7**, 289–292 (1989).
[30] G. Guderley, "Starke kugelige zylindrische Verdichungsstösse in der Nähe des Kugelmittelpunktes bzw. der Zylinderachse," Luftfahrtforschung **19**, 302–321 (1942).
[31] K. P. Stanyukovich, *Unsteady Motion of Continuous Media* (Gostekhizdat, Moscow, 1955), pp. 804–878.
[32] H. Schlichting, *Boundary-Layer Theory*, McGraw-Hill Series in Mechanical Engineering (McGraw-Hill, 1979).
[33] D. Isola, A. Guardone, and G. Quaranta, "Arbitrary Lagrangian Eulerian formulation for two-dimensional flows using dynamic meshes with edge-swapping," J. Comput. Phys. **230**, 7706–7722 (2011).
[34] D. Isola, A. Guardone, and G. Quaranta, "Finite-volume solution of two-dimensional compressible flows over dynamic adaptive grids," J. Comput. Phys. **285**, 1–23 (2015).
[35] G. Ben-Dor and K. Takayama, "Application of steady shock polars to unsteady shock wave reflections," AIAA J. **24**, 682–684 (1986).
[36] K. Takayama and M. Sasaki, "Effects of radius of curvature and initial angle on the shock transition over concave and convex walls," Rep. Inst. High Speed Mech. **46**, 1–30 (1983).
[37] F. Vignati and A. Guardone, "Dynamics of cylindrical converging shock waves interacting with aerodynamic obstacle arrays," Phys. Fluids **27**, 066101 (2015).
[38] D. C. Montgomery and G. C. Runger, *Applied Statistics and Probability for Engineers*, 5th ed. (John Wiley & Sons, 2010).
[39] F. Vignati and A. Guardone, "Multi-domain simulations of shock wave interaction with aerodynamic obstacles in cylindrical implosions," J. Comput. Appl. Math. **283**, 218–227 (2015).
[40] A. Guardone, D. De Santis, G. Geraci, and M. Pasta, "On the relation between finite element and finite volume schemes for compressible flows with cylindrical and spherical symmetry," J. Comput. Phys. **230**(3), 680–694 (2011).
[41] A. M. Tesdall, R. Sanders, and B. Keyfitz, "Self-similar solutions for the triple point paradox in gasdynamics," SIAM J. Appl. Math. **68**(5), 1360–1377 (2008).
[42] T. C. J. Hu and I. I. Glass, "Blast wave trajectories from height of burst," AIAA J. **24**, 607–610 (1986).